



Gamma cascades in gadolinium isotopes

Peter Grabmayr^a

Physikalisches Institut, Eberhard Karls Universität Tübingen, Auf der Morgenstelle 14, 72076 Tübingen, Germany

Received: 19 December 2022 / Accepted: 9 May 2023 / Published online: 27 May 2023
© The Author(s) 2023

Abstract The compound nucleus model is employed to calculate the γ decay after neutron capture by the gadolinium isotopes ^{155}Gd and ^{157}Gd . The respective γ cascades are analyzed for possible use in rare-event searches like $0\nu\beta\beta$ decay as neutron-veto for neutron energies in the range from 0.1 keV to 10 MeV.

1 Introduction

Neutrinos are elusive particles, however of great interest in astro- and particle physics and cosmology. Since many of their properties are still unknown, large-scale experiments and rare-events searches are setup or being devised. In some way also the neutrons are involved in these experiments either as background or as (intermediate) sensor, e.g. via the inverse β decay or Cherenkov light production after capture.

Also neutrons are difficult to detect due to their missing charge; they need to interact first with other nuclei producing charged particles. Since they are abundantly produced in natural decays or by cosmic radiation, thus in general, they are a nuisance producing backgrounds. Moderators and absorbers set around the actual sensitive volumes are standard since long times. Nowadays, these volumes are instrumented thus efficiently improving the signal versus background ratio.

Gadolinium is known for its extremely high absorption cross section at thermal neutron energies (~ 0.025 eV). In particular the odd isotopes with mass $A = 155$ and 157 contribute strongly, despite their combined abundance in natural gadolinium amounts only to $\sim 30\%$ [1]. For this reason gadolinium is widely used for passive shielding of thermal neutrons or to actively enhance the neutron detection. Gadolinium is often deployed when neutron tagging is involved in neutrino experiments [2–9]. Also an air shower experiment [10] has deployed Gadolinium. Gadolinium neu-

tron capture therapy is another, actual medical application. Apart from the photons, the internal conversion electrons are the main producer of the electron–hole pairs responsible for the energy transfer in the semiconductor type monitor. Also therefore, the γ spectrum must be well known for a clear separation of signals from internal conversion of photon interactions [11, 12].

The above mentioned experiments mostly imply thermal neutron capture. Cosmic radiation however is known to produce also high energetic neutrons of several tens of MeV kinetic energy, possibly in the vicinity of the sensors or within the active volume with small chances for thermalization. Albeit with lower probability, but possibly not negligible in rare-event searches, these neutrons might excite nuclei even at such energies where particle emission is energetically permitted. This way isotopes might be produced whose decay give signals emulating the ones searched for. Also the γ cascades might change since higher momenta transfer allow to populate other intermediate states. In rare-event searches at underground locations the muon flux in general is known. However, the neutron flux produced by cosmic radiation or by (α, n) reactions due to the decay within the natural decay chains is much less known; much less its energy distribution. Rare-event searches must not miss the further small chance that the muon veto has not responded and a fake signal might be produced.

GEANT4[13] is widely used in medical and in physics applications to simulate the reactions within the active volumes and the structural materials. However, it seems that the data base for neutron capture on gadolinium is not complete (see e.g. Refs. [14, Fig. 2], [15, Fig. 5]). Thus, other procedures have been developed including dedicated experiments for verification [8, 14–17]. These measurements aim at the determination of the γ cascades and of the feeding of intermediate states. In 2021 a new model for photo-nuclear reactions has been implemented in GEANT4.v11 [18].

^ae-mail: grabmayr@uni-tuebingen.de (corresponding author)

The $0\nu\beta\beta$ experiment GERDA at Gran Sasso underground laboratories has been completed with a total exposure of $\mathcal{E} = 127.2$ kg year [19]. The experiment remained “background free” resulting in a limit for the half life of neutrinoless double beta decay $T_{1/2}^{0\nu} = 1.8 \times 10^{26}$ year at 90% C.L. GERDA is the only one of the leading $0\nu\beta\beta$ experiments where half life $T_{1/2}^{0\nu}$ and sensitivity \mathcal{S} agree well. The follow-up experiment LEGEND aims towards $\mathcal{S} = 10^{28}$ year by enlarging the active mass towards the tonne-scale [20,21]. Being a factor 25 larger calls for additional measures in reducing the possible background induced by neutrons in order to keep the proposed experiment “background free” as well. In particular the production of the isomer ^{77m}Ge might be an unwanted source of signal-like events. Simulations [22] have shown that ^{77m}Ge can be produced by neutrons with energies up to 1 MeV. A good understanding of the feeding of all the intermediate states and their γ decay is of great importance for designing background reductions schemes in hardware and in software. For LEGEND, this holds for Germanium as well as for Gadolinium.

The present work aims at a complete description of the γ decay after neutron capture on gadolinium up to neutron energies of about 10 MeV, however focusing on the epithermal region. Internal electron conversion or β decay will not be considered. The produced γ cascades will serve as input for Monte Carlo simulations of realistic setups, e.g., the LEGEND-1 tonne [20]. MAURINA is a computer code developed by Mario Uhl [23] as a follow-up of STAPRE. This paper describes the models used in the code (Sect. 2) as well as the relevant input parameters (Sect. 3). The reproduction of the experimental cross sections is demonstrated in Sect. 4. The resulting γ spectra and multiplicities are shown for various parameter sets in Sect. 5 and compared to published results. A summary is given in Sect. 6.

2 The models within MAURINA

The code MAURINA [23] has been developed by Mario Uhl in the Nineties as expansion of the Hauser-Feshbach code STAPRE [24]. MAURINA contains all the necessary routines and is not dependent on any output from other programs. It was written in FORTRAN-IV and it contains about 47,000 lines. For the present purpose the code has been adapted to modern compilers (GNU Fortran 7.5); some arrays have been expanded, e.g., to account for 198 instead of 50 discrete states for each of the final nuclei. All input is read from one file. Results can be stored in ROOT or ENDF6 format.

The code MAURINA provides several choices for the cross section calculations. Here, only the ones used in this work are listed below:

1. compound nucleus model with the formalism according to Hauser–Feshbach (HF) [25].
2. width-fluctuation correction for low energies [26].
3. level densities according to the back-shifted Fermi-gas (FG) model [27–29], or to a semi-empirical model considering shell effects [30]
4. spherical optical model for the calculation of particle transmission coefficients [31–35].
5. pre-compound model by Kalbach [36].

The present calculations have been performed with the Hauser–Feshbach mode as the basic model in order to calculate the formation and decay of the compound nucleus and its daughter nuclei. The formation is determined by the angular momentum (l) dependent transmission coefficients $T_l(E)$ of the projectile with respect to the target nucleus at energy E . These coefficients are calculated from the spherical optical model. The cross section for formation of the compound nucleus can be calculated by

$$\sigma_c^l(E) = \pi\lambda^2 (2l + 1) \cdot T_l(E) \quad (1)$$

where E is the transition energy and λ the corresponding wave length. All possible l values have to be considered when forming the compound nucleus with spin and parity J^π . The compound nucleus is assumed to lose all information regarding the entrance channel α due to thermalization and thus factorizes

$$\sigma_{\alpha,\beta}(E) = \sigma_\alpha(E) \cdot P_\beta \quad \text{with} \quad (2)$$

$$P_\beta = T_\beta / \sum_{i=J,l,\pi,E_i} T_i \quad (3)$$

where $\sigma_\alpha(E)$ is the formation cross section of the compound nucleus and P_β the probability for the decay into channel β . Employing time reversal and reciprocity [37] the above Eq. 1 can be used also for the decay back into the ground state or to an excited state considering proper summation over all spin and angular momentum couplings. For high incoming energies the decay into different particle channels has to be taken into account. Considering the decay from or to high excitation energies in the residual nucleus the large number of levels is taken into account via the respective densities $\rho(E_i, J_j^\pi)$ [27–30,38].

3 Selection of model parameters

This work concentrates on the γ decay after neutron capture on the two gadolinium isotopes ^{157}Gd and ^{155}Gd . Thus, special care for the parameters relevant to ^{158}Gd and ^{156}Gd was taken. Several parameters have been adapted from the calculations shown in Ref. [39]. Masses and Q values are taken from Ref. [40].

Table 1 Optical model potentials for the particle transmission coefficients

Particle	Acronym	References
Neutron	McEllistrem+	[31]
Proton	MANI-MELK	[32]
Deuteron	PEREY	[33]
Triton	BECGRE	[34]
Helion	BECGRE	[34]
α	MOD MCFAD	[35]

Table 2 Lorentzians for ^{156}Gd and ^{158}Gd determining the photon strength functions [39]

Multipole	Energy [MeV]	Width [MeV]	Cross section [mb]
^{156}Gd			
M1	7.62	4.00	2.03
E1 (1)	3.00	1.00	0.40
E1 (2)	11.20	2.60	180.00
E1 (3)	15.20	3.60	242.00
E2	11.70	4.24	3.69
^{158}Gd			
M1	7.58	4.00	1.79
E1 (1)	3.10	1.00	0.35
E1 (2)	11.70	2.60	165.00
E1 (3)	14.90	3.80	249.00
E2	11.65	4.21	3.66

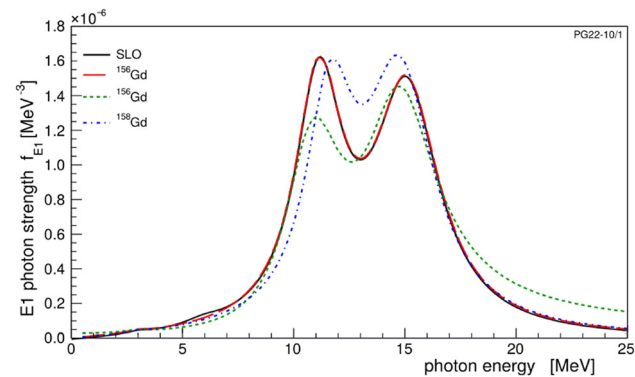


Fig. 1 The E1 strength functions f_{E1} for ^{156}Gd (red, long-dashed, 3LO) and ^{158}Gd (blue, dot-dashed) are presented. f_{E1} for ^{156}Gd (SLO) calculated by Ref. [16] using 4 resonances (black, full) compares well. An energy and temperature dependent width (green, dashed; ALO) was suggested by M. Uhl [39]

Transmission coefficients

The transmission coefficients are calculated from standard optical potentials as shown in Table 1. The spherical optical potentials have been used despite the fact that several nuclei are deformed.

The neutron optical potential had been taken as it was modified by Ref. [39] in its imaginary amplitude by a factor

1.25 for improved reproduction of the total cross section. The parameters for the α potentials have been slightly modified for calculations at higher energies, which is of no relevance in the present work. The mass and energy dependence of the parameters is implemented as given in the literature.

The photon strength functions

Calculating the photon decay MAURINA considers the six strength functions f_{XL} for M1, E1, E2, M2, E3, and M3 radiation. The strengths of the last three types were taken from the single-particle model with 1 Weisskopf Unit/MeV. For the first three types the strength functions are modeled by resonances formed by up to 3 Lorentzians as specified in detail in Table 2 and shown in Fig. 1.

The transmission coefficients $T_{XL}(\epsilon_\gamma)$ for multipole type XL are related to the respective strength functions $f_{XL}(\epsilon_\gamma)$ by

$$T_{XL}(\epsilon_\gamma) = 2\pi \epsilon_\gamma^{2L+1} f_{XL}(\epsilon_\gamma) \tag{4}$$

where the γ -transition energy is denoted by ϵ_γ .

The E1 strength is the dominant one in the decay after neutron capture at low neutron energies. The comparison of f_{E1} for ^{156}Gd shows that the differences between this work with 3 resonances and that of Ref. [16] with 4 resonances is marginal. However, there is a clear difference between the two gadolinium nuclei ^{156}Gd and ^{158}Gd . Also applying the energy and temperature dependence of the width of the Lorentzians (ALO) – as suggested by Ref. [41] and employed for Gd by Uhl [39] – increases the tails and dampens the resonance peaks.

The experimental levels

The energies, spins and parities of the ground and excited states are taken from the most recent compilations of the Nuclear Data Sheets [42,43]. In some cases spin and parity had to be assumed. Up to ten branching ratios for each level can be given. In case the compilation did not provide any experimental values, these are taken from calculations using the strength functions mentioned above. The ten strongest branchings are selected. For ^{158}Gd 196 level up to 3.65 MeV have been entered, and 198 up to 2.81 MeV for ^{156}Gd , respectively.

Levels in the continuum

At higher energies the experimental information on individual levels gets sparse and/or inaccurate. The number of levels rises strongly with excitation energy as can be seen in Figs. 2 or 3. Thus the energy region between the highest experimental level and the maximum excitation energy defined by the incoming neutron energy is divided into bins. Equal widths are taken except close to both ends of the continuum or around particle thresholds, where a finer binning can be chosen. Always the maximum number bins has been used as there is a slight dependence of the results on the binning.

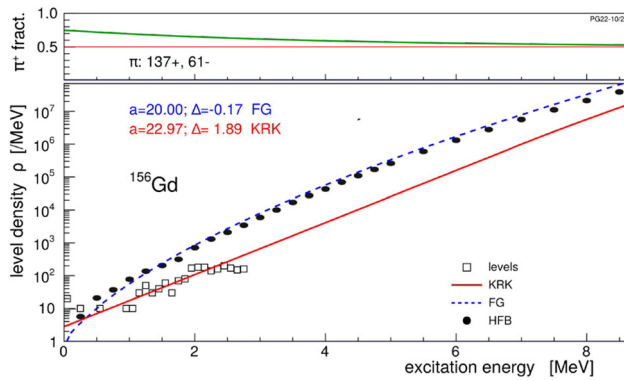


Fig. 2 Binned experimental levels (open squares) of ^{156}Gd in comparison to the HFB predictions [38] (full dots) and the level densities calculated by MAURINA for the back-shifted Fermi Gas (FG) and the empirical (KRK) models are shown in the lower panel. The upper panel shows the fraction of positive parity states per bin. A bin width of 100 keV was chosen

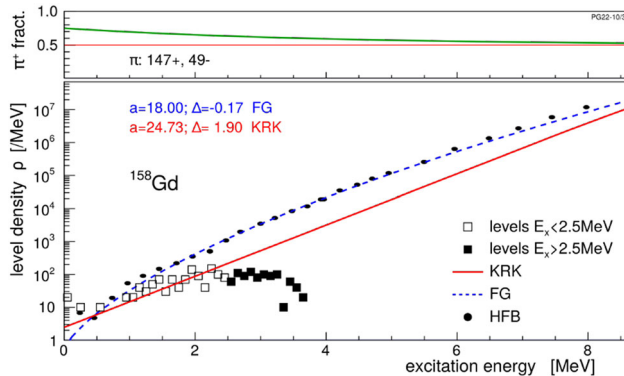


Fig. 3 Same as Fig. 2 but for ^{158}Gd

Several models for the calculation of the level density are available in the code MAURINA. Two out of the 9 models have been employed: (i) the empirical one by Kataria et al. (KRK) [30] considering deformation and shell effects and (ii) the standard back-shifted Fermi-Gas (FG) model in the formulation by Lang [44] with the two parameters a for the level density and Δ for the energy shift towards a fictive ground state, respectively, are used in this work for comparison.

The KRK model had been used for the description of several Gd isotopes in Ref. [39] and is adapted for the present purpose. The FG model has been chosen to reproduce the level densities calculated by Ref. [38] and shown in binned form in Refs. [16, 17]. Figures 2 and 3 show the quality of fit (black dots and blue dashed line) and the respective parameters for ^{156}Gd and ^{158}Gd . In Table 3 these parameters are compared with those from literature. It is noticed that these values differ quite a bit, less for ^{158}Gd .

A further comparison with experimental data sheds more doubts on the HFB nuclear level densities. The experimentally known levels given in Refs. [42, 43] are taken into bins of 100 keV (squares) and are plotted as function of excita-

Table 3 Comparison of level density parameters for the back-shifted Fermi gas model

	^{156}Gd		^{158}Gd	
	a	Δ	a	Δ
This fit	20.00	-0.17	18.00	-0.17
Dilg [27]	18.14	0.15	17.83	0.28
Egidy [28]	18.45	0.36	17.91	0.28

tion energy for ^{156}Gd (Fig. 2) and ^{158}Gd (Fig. 3). In contrast to the HFB model the KRK parameterization describes the increase of level density quite well for ^{156}Gd . However, for ^{158}Gd only up to ~ 2.3 MeV there is agreement. Most likely, some experimental information is still missing above that energy. The difference between the HFB/FG parameterization and the KRK is smaller for ^{158}Gd than for ^{156}Gd .

The upper parts in Figs. 2 and 3 display the fraction of positive parity states as function of excitation energy. The numbers represent the respective counts for positive and negative parity within the first 198 levels in those nuclei as given in Refs. [42, 43]. The parity fractions can be kept constant (π^c) or may decay and equilibrate via an exponential decrease up to ~ 8 MeV (π^d).

The exciton model

The exciton model with standard parameterization is used. The multiplier for the internal transitions is set to 150 MeV^3 [45].

The energy scale

The maximum neutron energy has been chosen to be 10 MeV to produce an entry above the Q -value for the (n,2n) reaction with $Q = 6.434$ and 6.359 MeV for ^{155}Gd and ^{157}Gd , respectively [40]. When 10 MeV neutrons impinge on ^{155}Gd there are 11 nuclei energetically reachable: $^{154, 155, 156}\text{Gd}$, $^{153, 154, 155}\text{Eu}$, $^{151, 152, 154}\text{Sm}$, ^{151}Pm and ^{148}Nd ; in case of ^{157}Gd these are just 9: $^{156, 157, 158}\text{Gd}$, $^{155, 156, 157}\text{Eu}$, $^{153, 154}\text{Sm}$ and ^{150}Nd .

In both cases, proton and α emission occur on a negligible level. The charged particles are hindered strongly due to their Coulomb barriers, even when the Q value is positive. However, helions and tritons are included to be consistent for the case of need for even higher neutron energies.

Calculations have been performed down to the lowest energy of 0.1 keV, reaching the epithermic region. However, an incoming neutron energy of 5 keV is chosen for comparison of the parameters.

4 The neutron capture cross sections

Having prepared the level densities and transmission coefficients to be used, neutron capture cross sections can be calculated and γ cascades can be produced via a Monte Carlo

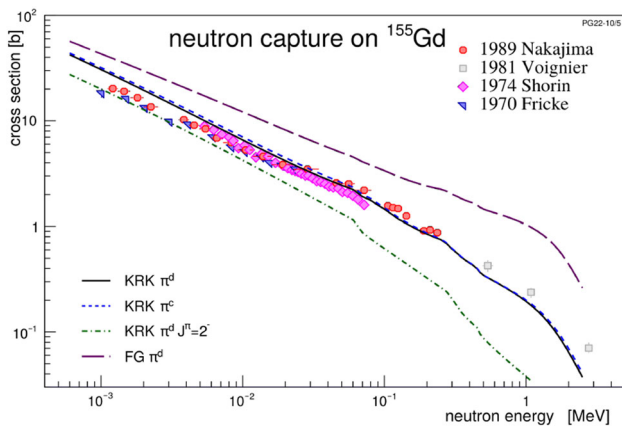


Fig. 4 The excitation function of the $^{155}\text{Gd}(n,\gamma)^{156}\text{Gd}$ reaction calculated by the KRK model with a constant (π^c , black full line) and a decaying (π^d , blue dashed line) parity distribution are compared to four experiments [46–49]. For comparison the green line shows that fraction going through the $J^\pi = 2^-$ compound states. The magenta dashed line gives the result for the FG parameterization

procedure within MAURINA. As reference the following data set is chosen: use of all experimental levels, f_{E1} with 3 Lorentzians (Table 2), the KRK model for level density in the continuum and an exponential decrease of the positive parity state fraction $\pi^+ = \pi^d$ from 0.75 to 0.5 as shown in Figs. 2 and 3. The choice of parameters is corroborated by the cross sections for the (n,γ) capture reactions on ^{155}Gd and ^{157}Gd , respectively.

The excitation functions of the neutron capture reaction on ^{155}Gd with the KRK model are displayed in Fig. 4 in

comparison with experiments [46–49]. The two KRK calculations differ only in the treatment of the parity fractions as function of excitation energy in ^{156}Gd . Both describe the data satisfactorily down to about 5 keV. At rather low energies the calculations overshoot the data. At these energies the data come closer to the line made by the fraction of those compound states with $J^\pi = 2^-$ (green, dot-dashed line) only. The n_TOF Collaboration [50] recently has measured the capture cross sections of ^{155}Gd and ^{157}Gd finding resonances up to 1 keV, however without spin assignment. Ref. [46] has found resonances up to 370 keV.

The other three parameterizations are off in scale by 50% at 5 keV incoming neutron energy as discussed later (Table 4). The FG calculation (dashed magenta) remains off very clearly also at high neutrons energies, while the others (not shown) converge with increasing energies.

A similar good description of experimental data is achieved for neutron capture on ^{157}Gd for the standard parameterization while showing the same discrepancies for the FG calculation. Again the cross sections at epithermic energies favors the assumption of $J^\pi = 2^-$ resonances. One notices, when replacing the higher experimental levels in ^{158}Gd (black dots in Fig. 3) by the level densities of the continuum, that the cross sections (red dotted line in Fig. 5) change only slightly. However, the γ cascades might be affected. Thus, the discussion in the following section will concentrate on capture on ^{155}Gd .

Table 4 The mean multiplicities M_m and cross sections $\sigma_{n\gamma}$ for the reaction $^{155}\text{Gd}(n,\gamma)^{156}\text{Gd}$ at 5 keV neutron energy for various parameterizations as discussed in Sect. 3. σ_n^p and σ_γ^p are the total production cross sections for neutrons and γ s, respectively. The cross sections are given in [b]. The lower part shows the results for $E_n = 1$ MeV and 10 MeV, respectively

Level dens.	f_{E1}	M_m	$\sigma_{n\gamma}$	σ_n^p	σ_γ^p
$E_n = 5$ keV					
KRK, π^d	3LO	4.59	10.52	11.13	40.06
KRK, π^c	3LO	4.60	11.16	10.49	51.14
KRK, π^d	ALO	4.20	5.64	14.22	25.56
1 exc., KRK, π^d	3LO	4.63	5.58	11.29	40.89
FG, π^d	3LO	5.00	17.91	3.74	88.95
$E_n = 1$ MeV					
KRK, π^d	3LO	5.19	0.195	5.50	9.90
KRK, π^c	3LO	5.19	0.202	4.49	9.92
KRK, π^d	ALO	5.18	0.086	4.61	9.56
1 exc., KRK, π^d	3LO	5.58	0.182	4.51	9.93
FG, π^d	3LO	5.59	1.038	3.66	12.70
$E_n = 10$ MeV					
KRK, π^d	3LO	6.62	1.68E−4	2.72	4.29
KRK, π^c	3LO	6.57	1.58E−4	2.72	4.29
KRK, π^d	ALO	6.48	1.30E−4	2.72	4.28
1 exc., KRK, π^d	3LO	7.12	1.64E−4	2.72	4.29
FG, π^d	3LO	7.30	1.30E−3	2.72	3.64

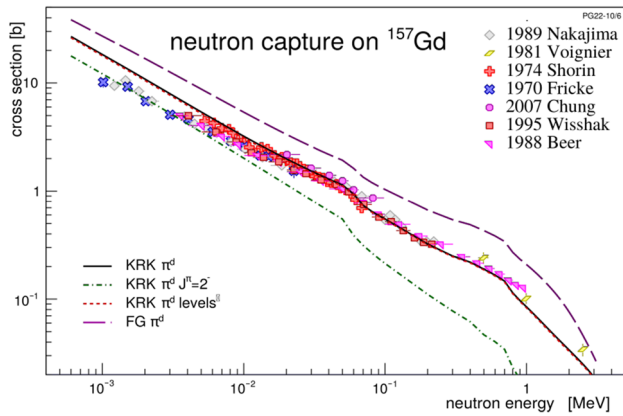


Fig. 5 The excitation function of the $^{157}\text{Gd}(n,\gamma)^{158}\text{Gd}$ reaction calculated by the KRK model with a decaying (π^d) parity distribution (black line) is compared to seven experiments [39,46–49,51,52]; the $J^\pi = 2^-$ fraction is shown by the green dash-dotted line, the calculation with a reduced number of levels by the red dotted line and the FG parameterization is shown by the magenta dashed line

5 The γ spectra from neutron capture

At a neutron energy of $E_n = 5$ keV the excitation function describes the capture data very well. The energy is low enough to guarantee the prevalence of s -wave capture. For each calculation shown in the following section 10^7 cascades were produced.

5.1 The (n,γ) reaction on ^{155}Gd

The 10^7 γ cascades after neutron capture on ^{155}Gd have been created with the standard parameters mentioned above. They are analyzed for the multiplicity and the sequence of decay. The top part of Fig. 6 shows the total γ spectrum as blue line on a logarithmic scale. The running sum is normalized to unity and shown as red line on a linear scale. These spectra have a binning of 1 keV. At low and high energies a plethora of discrete transitions are clearly visible. They are sitting on a broad continuum. Due to secondary interactions in the various media most of the peaks will be indiscernible in experiments except for extreme resolution.

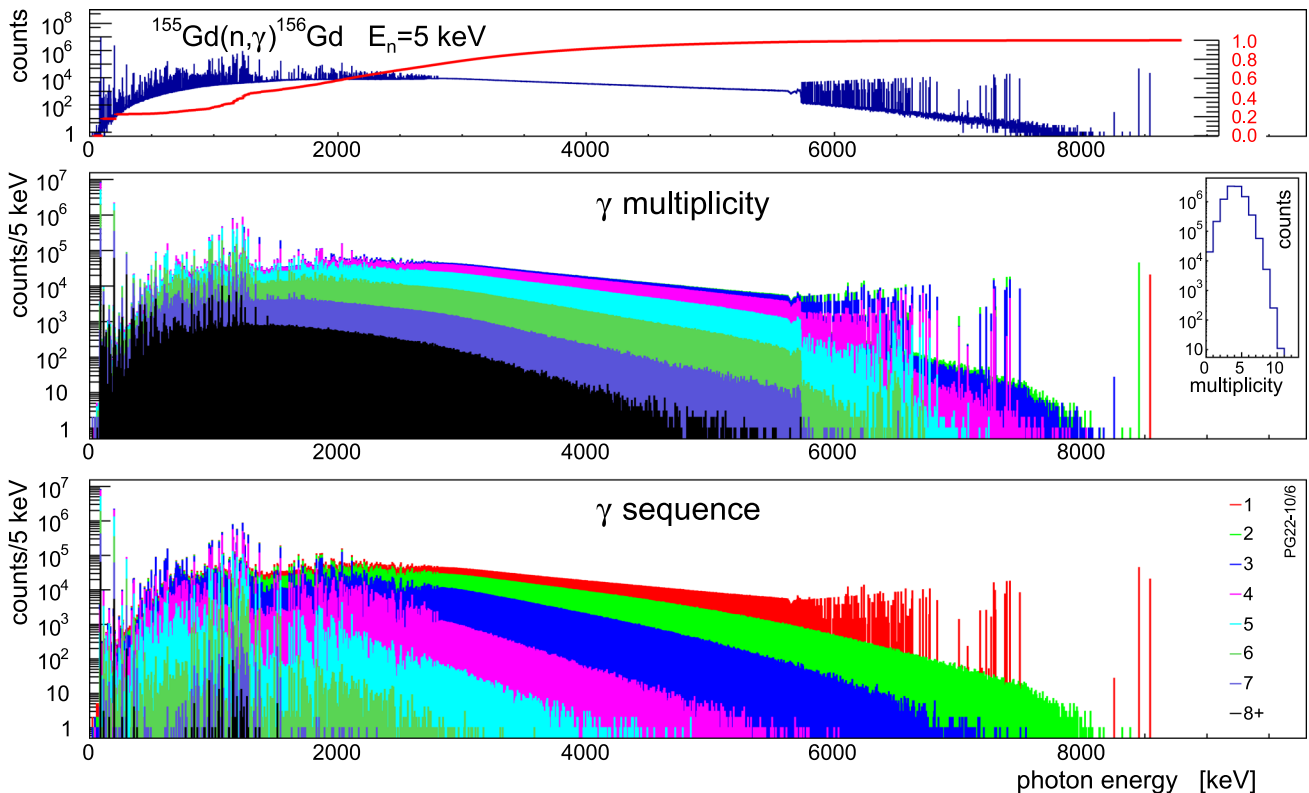


Fig. 6 The γ -cascades from (n,γ) on ^{155}Gd employing the standard parameterization. Top: the total γ spectrum in ^{156}Gd and the running sum normalized to 1 (red line). Middle: the stacked spectrum for the multiplicities M ; the inset shows the distribution of multiplicity M .

Bottom: the sequence of γ -quanta within the cascade. The color code is valid for the middle and bottom graph. 8+ indicates that all higher entries have been added

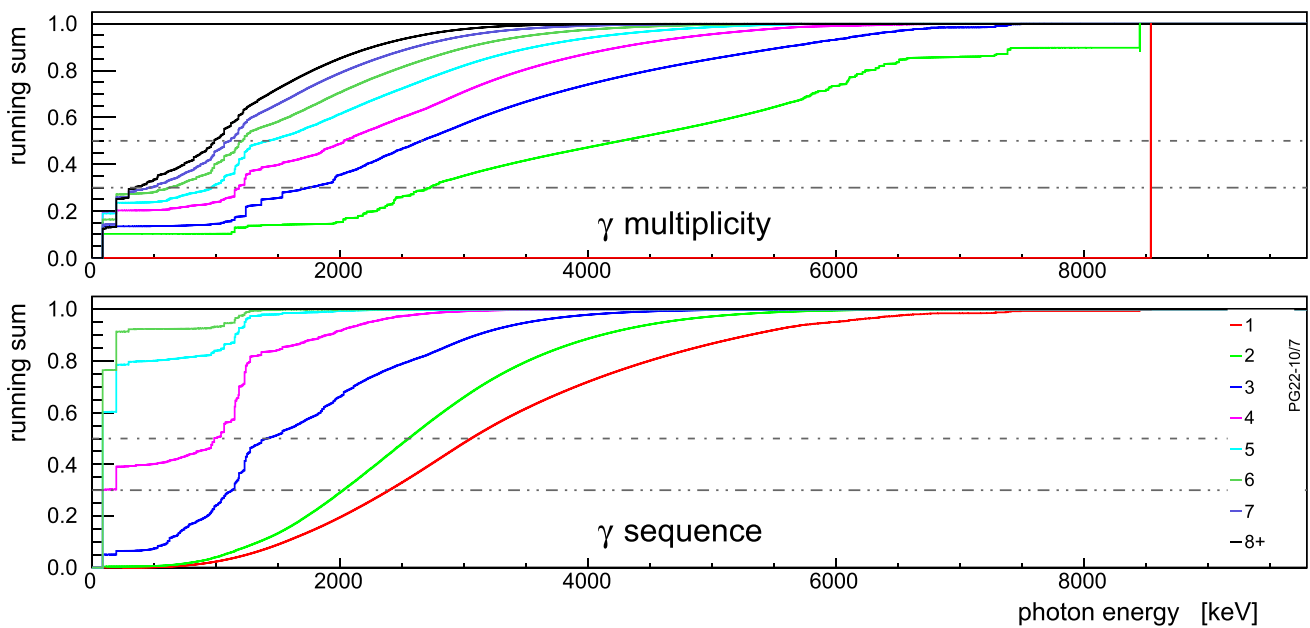


Fig. 7 The running sums for multiplicity and γ -sequence spectra shown in Fig. 6

The middle part of Fig. 6 displays the multiplicity distribution as histogram in the inset and the respective spectra in stacked form in the main graph. For the latter a binning of 5 keV was employed. The multiplicity $M = 1$ is connected solely with the ground state transition (red line, for the color code refer to the bottom panel). Its intensity is 0.9% of the total spectrum. The highest photon energy found for $M = 2$ is provided by the transition to the first excited state combined with a rather low photon, however also other combinations are observed. One notices that with higher M the direct transitions to the low lying levels decrease – corresponding to high γ energies –, while the transitions between the levels become more important as observed in the low energy part of the γ spectrum. The mean multiplicity amounts to $M_m(\text{KRK}) = 4.59$.

The individual γ s can be ordered by their occurrence within the cascade as shown in the bottom panel. Again, a binning of 5 keV was applied. One realizes, that the low lying discrete levels are populated primarily by the first γ in the cascade. The secondary and following γ s produce spectra each being smooth above $E_\gamma \sim 3$ MeV. The structures at $E_\gamma < 2.81$ MeV belong to transitions between the discrete levels.

For multiplicity and sequence spectra the respective running sums have been normalized to 1. They are displayed in Fig. 7. For Veto purposes it might be interesting to understand what fraction of γ s has passed a defined energy threshold. Thresholds of 30% and 50% are indicated in the two graphs. It is noticed, the higher the multiplicity or the later in the sequence a γ occurs the faster a fixed threshold is surpassed.

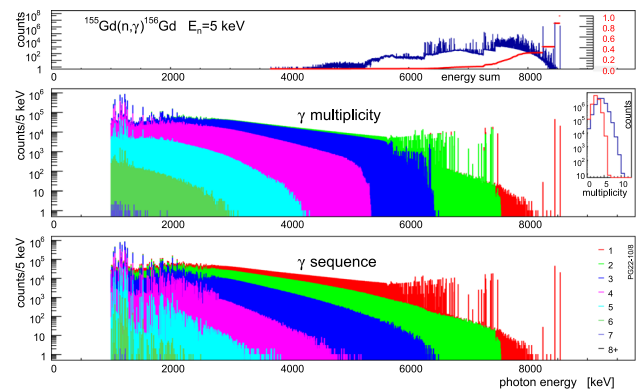


Fig. 8 The γ spectra from the $^{155}\text{Gd}(n,\gamma)^{156}\text{Gd}$ reaction after applying a cut at $E_\gamma^i = 1$ MeV (same notation as in Fig. 6)

Thresholds and cuts

In experiments there always will be a certain electronic threshold, in some cases also a physical motivated one, e.g., for Cerenkov light production by the γ s in water. Exemplifying, a cut on individual γ s with $E_c = 1$ MeV is applied, and the change in spectra for multiplicity and sequence is shown in Fig. 8. A direct comparison to Fig. 6 is in order, except for the top panel, where summed energy is displayed. The maximum multiplicity decreases strongly as seen in the inset of the middle panel and thus the centroid. The upper ends of the consecutive multiplicity spectra differ just by 1 MeV, whereas those of the sequence spectra increases with each step. The respective running sums saturate at much lower energies than shown in Fig. 7.

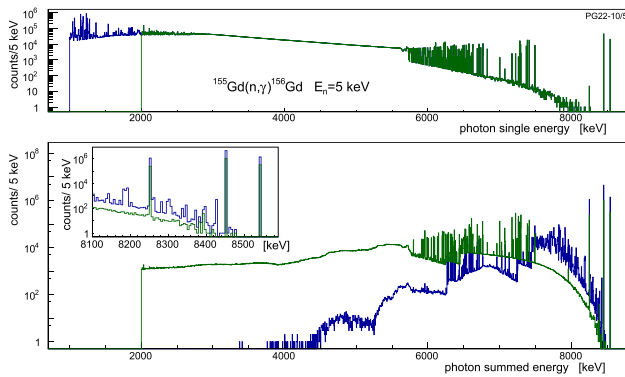


Fig. 9 The γ spectra from the $^{155}\text{Gd}(n,\gamma)^{156}\text{Gd}$ reaction after applying a cut at $E_{\gamma}^i = 1$ MeV (blue) and 2 MeV (green), respectively. Top: spectrum of the single γ energies; Bottom: spectra of the summed energy; the inset shows the expanded top region

For demonstration the effects of cuts of $E_c = 1$ MeV and 2 MeV, respectively, are demonstrated. Figure 9 (top) displays the spectrum of individual γ s. The cut of $E_c = 1$ MeV (blue) removes 30% of the low energetic γ s, but still retains all cascades. In contrast, $E_c = 2$ MeV (green) removes 58% of the γ s while keeping 99,7% of the cascades. In the bottom graph of Fig. 9 the summed energy of each cascade is shown with the inset giving an expanded view of the top region. A strong direct population of the low lying discrete states is observed, even stronger for the lower cut. The lower cut allows higher sums within a single cascade, thus the median γ energy is higher for $E_c = 1$ MeV. The bumpy structure of a width of about 1 MeV reflects the threshold (blue histogram) whereas the cut $E_c = 2$ MeV produces less marked structures (green histogram).

Other parameterizations and higher energies

In Sect. 3 the level density parameterization according to the Fermi gas model has shown a lesser agreement with the experimental data, but fits those provided by Ref. [16]. As shown in Fig. 4 also the cross sections cannot be reproduced. On the other hand, the resulting cascades show similar gross features. The average multiplicity amount to $M_m(\text{FG}) = 5.00$. This seems only a small difference to $M_m(\text{KRK})$, however averages are hiding details. Still, the smallness of difference can be explained by the fact that (i) the increase intensity with excitation energy is similar and (ii) only relative populations of states are finally relevant. Similarly, when using the energy dependent $E1$ strength (ALO) or removing the experimental levels (except for one fictive excited state at $E_x = 1$ keV) or keeping the ratio between positive and negative parity states constant at $\pi^c = 0.75$, the mentioned patterns remain roughly the same within the spectra.

As understood from Fig. 4 and as can be seen in Table 4, the cross sections differ quite strongly due to different absolute level densities at the excitation energy in the compound

nucleus defined by the incoming neutron energy. Also the f_{E1} strength function changes the decay pattern.

Table 4 shows for various parameterizations the mean multiplicity M_m , the capture cross sections $^{155}\text{Gd}(n,\gamma)^{156}\text{Gd}$, and σ_n^p and σ_{γ}^p , the total production cross sections for neutrons and γ s, respectively. These data are given for three neutron energies of $E_n = 5$ keV, 1 MeV and 10 MeV, respectively. For the lowest energy, the numbers differ from each other in every aspect. While M_m for the (KRK, π^d , 3LO) and (KRK, π^c , 3LO) models are almost the same, the constant parity ratio produces more photons as seen in (n, γ) and σ_{γ}^p . In contrast the other two KRK variants are lower in M_m and (n, γ). The FG parameterization produces γ s at the expense of neutrons. At $E_n = 1$ MeV one recognizes a certain grouping of the results which at 10 MeV clearly distinguishes the KRK and FG parameterization. At higher neutron energies more particle channel open up, thus allowing for more neutrons and/or γ s to be emitted while the capture reactions becomes negligible. The cross sections of the capture process at 10 MeV coincide for the KRK model, however disagree much stronger from the FG model than at low neutron energies. This is clearly an effect of the different level density. However, the production cross sections σ_n^p and σ_{γ}^p , respectively, are indistinguishable; they are about 4 orders of magnitude larger than the (n, γ) process. The multiplicities increase moderately with incident neutron energy. They differ even at 10 MeV for the different model assumptions. Tuned parameters for the residual nuclei other than ^{155}Gd might change the absolute numbers for σ_n^p and σ_{γ}^p at higher energies but the general pattern will remain.

At energies up to the threshold for the (n,2n) reaction ($Q_{n,2n} = 6.434$ MeV) the spectra look like stretched versions of Fig. 6. Figure 10 demonstrates the changes in the γ spectra after neutron capture for incoming neutron energy of 10 MeV, well above $Q_{n,2n}$. For $E_n = 10$ MeV one notices in the spectrum a reduction of the direct population of the lowest state and an increase at low energies due to the transitions between the discrete states.

The dominant channels are elastic and inelastic neutron scattering. Due to the Coulomb barrier the other channels are strongly suppressed even at 10 MeV. The $^{155}\text{Gd}(n,p)^{155}\text{Eu}$ reaction as the strongest of those with charged reaction products is on the level of mb, similar in size to the capture reaction. Neutrons and γ s are produced by a factor 10^4 more abundantly than any charged particle. The fraction of pre-equilibrium reactions amount to 14% at 10 MeV incident energy, less than 1 permille at 1 MeV respectively.

The spin dependence of the γ decay

For a better understanding of the results the population of the involved states in the compound nucleus are shown in Fig. 11 for two energies, namely $E_n = 5$ keV and 10 MeV, respectively. The absolute population (dashed lines), where

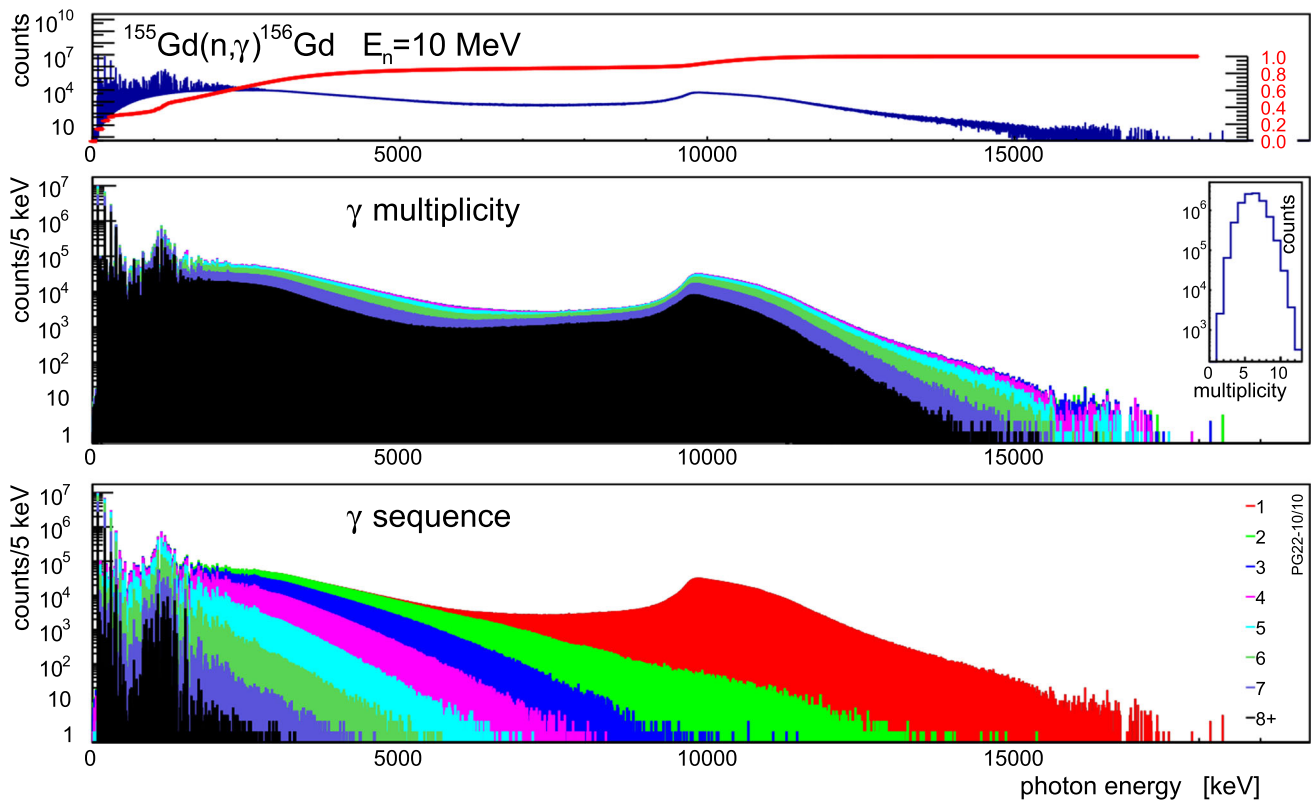


Fig. 10 γ -cascades from (n, γ) on ^{155}Gd according to the standard parameterization, the same as Fig. 6 but for an incident neutron energy of 10 MeV

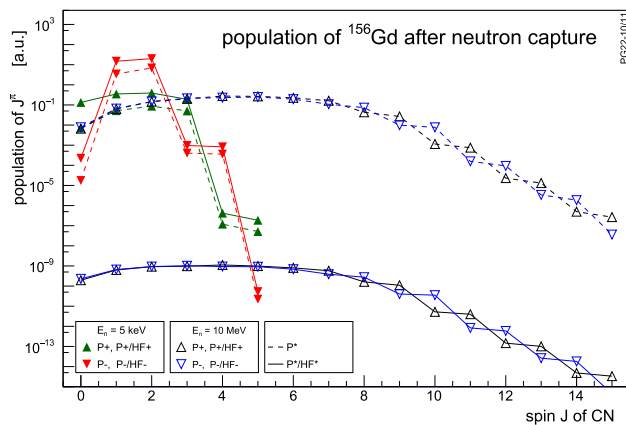


Fig. 11 The population of the states with J^π in the compound nucleus ^{156}Gd after the $^{155}\text{Gd}(n, \gamma)^{156}\text{Gd}$ reaction with neutron energies of $E_n = 5$ keV and 10 MeV, respectively

the arbitrary units are equal to barns, is differentiated for spin and parity of the compound states as well the ones normalized by the Hauser–Feshbach denominator (full lines). As expected, the s -wave character of the capture process prevails at the low energy. Starting from $J^\pi = 3/2^-$ in ^{155}Gd the coupling rules allow only $J^\pi = 1^-$ and $J^\pi = 2^-$ states in ^{156}Gd to be reached by $\ell = 0$. Figure 11 indicates that regarding the population of CN states there is almost no dif-

ference to thermal capture as long as the assumption of a statistical process holds. Other ℓ transfers contribute at least 4 orders of magnitude less. The positive parity states (green) are more evenly distributed than the negative ones (red). The relative small differences between the dashed and the full lines are a result of the prevalence of γ decay. The picture is quite different for $E_n = 10$ MeV. The distributions are wide and smooth. Differences between positive and negative parity states appear only for rather high J . The normalization by a factor $\sim 10^9$ shows that capture is a minor channel at incoming energy of 10 MeV or equivalently at excitation energy of about 18 MeV for ^{156}Gd .

Selecting a specific compound state within the code allows one to emulate the γ decay of resonances in the thermal region. At $E_n = 5$ keV the $J^\pi = 1^-$ and $J^\pi = 2^-$ states are produced with 3.06 b and 6.28 b, respectively; in sum the two states amount to 98% of the total capture cross section. At $E_n = 10$ MeV their contributions amount to 8% only.

In Fig. 12 the multiplicities of the γ cascades are shown for the two selected states $J^\pi = 1^-$ and $J^\pi = 2^-$ and the two neutron energies $E_n = 5$ keV and $E_n = 10$ MeV, respectively. In addition, the multiplicity distributions for $J^\pi = 10^{+/-}$ are given. All are normalized by the respective sum. The distributions differ marginally for the two states $J^\pi = 1^-$ and 2^- , but the higher energy broadens and shifts

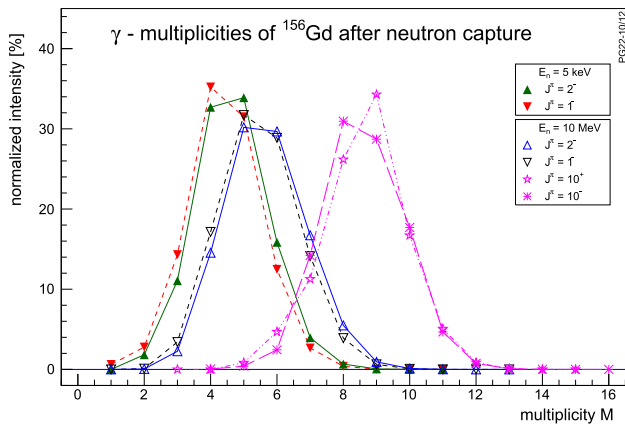


Fig. 12 Normalized γ multiplicities in percent after the $^{155}\text{Gd}(n,\gamma)^{156}\text{Gd}$ reaction with neutron energies of $E_n = 5$ keV and 10 MeV, respectively, separately for the compound states with $J^\pi = 1^-, J^\pi = 2^-$ and $J^\pi = 10^{+/-}$

them by one unit. In contrast, a clear shift is observed for the decay from both the $J^\pi = 10^{+/-}$ states.

The similarity in multiplicities of the two states $J^\pi = 1^-$ (red) and $J^\pi = 2^-$ (blue, middle graph) is astounding. Therefore, the γ cascades for the two states are compared in

Fig. 13 between themselves and to the FIFRELIN results [8] at thermal energies. The most notable differences between cascades starting from $J^\pi = 1^-$ or $J^\pi = 2^-$ are the relative transition rates to the ground and first excited state. For $J^\pi = 1^-$ almost equal rates are observed while the decay from the $J^\pi = 2^-$ compound state favors the first excited state, which is a 2^+ state, over the 0^+ ground state by a factor 10^4 . This can be easily related to the relative strengths of $E1$ over $M2$ transitions. The top graph of Fig. 13 displays the ratio of the two γ spectra showing further discrepancies are to be found mostly at the low and high end of the spectra. Note, that the multiplicities do not reflect these differences.

The code FIFRELIN is specially designed for calculating the fission process at thermal energies [53] and it is not a full-fledged Hauser–Feshbach code dealing with higher excitation energies. The authors [8] have provided a file with 10^7 γ cascades after neutron capture on Gadolinium. For these calculations they had assumed the capture to proceed via a $J^\pi = 2^-$ compound state. Out of these cascades 63% have just one additional electron emitted with 89 keV, the transition from the first excited to the ground state. 1.4% are with other single electron emission and 4.9% of the cascades contain two or more electrons; this leaves 31% cascades with γ s

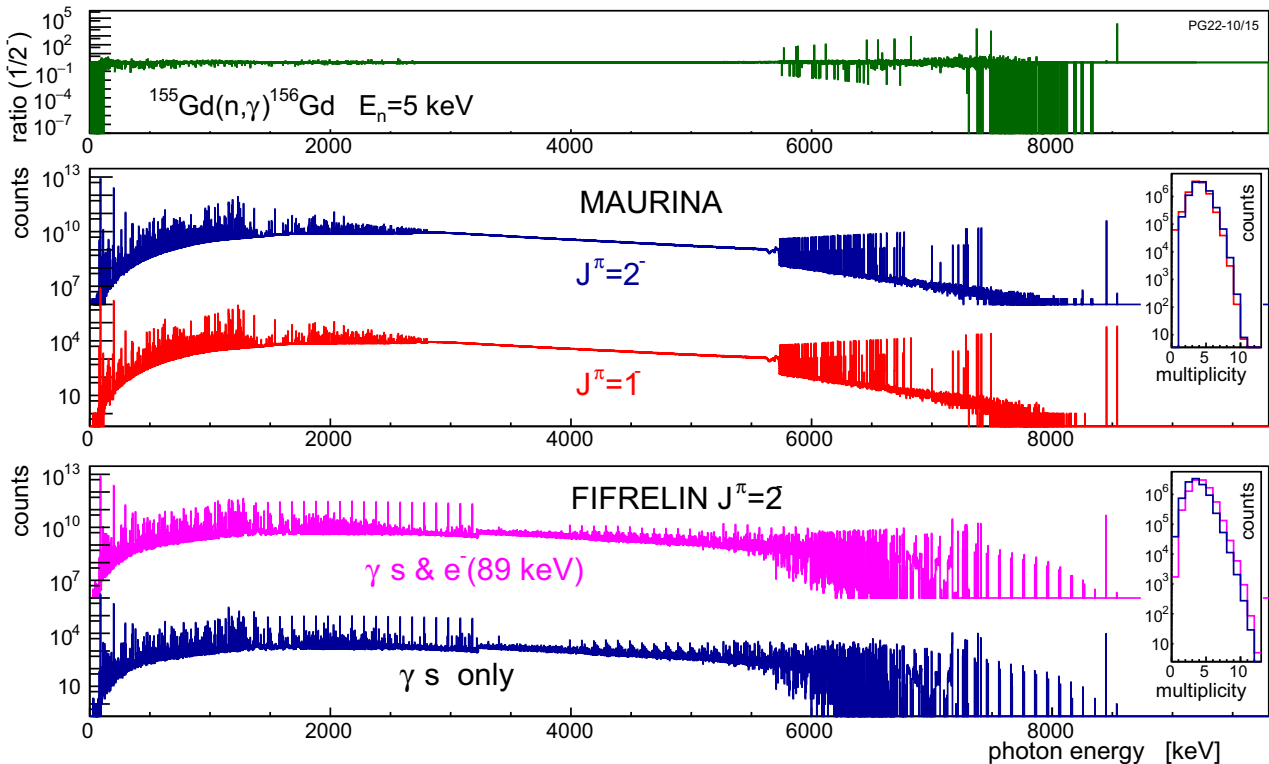


Fig. 13 γ -cascades from (n,γ) on ^{155}Gd separately for compound nucleus spins $J^\pi = 1^-$ and 2^- in comparison to those from FIFRELIN [8] and the respective multiplicities (insets). Bottom: spectra for $J^\pi = 2^-$ by FIFRELIN selecting γ s only and (with offset of 10^6) for γ s

and the electrons from the first excited state at 89 keV; Middle: spectra for $J^\pi = 1^-$ and 2^- by MAURINA. Note the offset of 10^6 for $J^\pi = 2^-$; Top: ratio of counts for $J^\pi = 1^-$ and 2^- from MAURINA

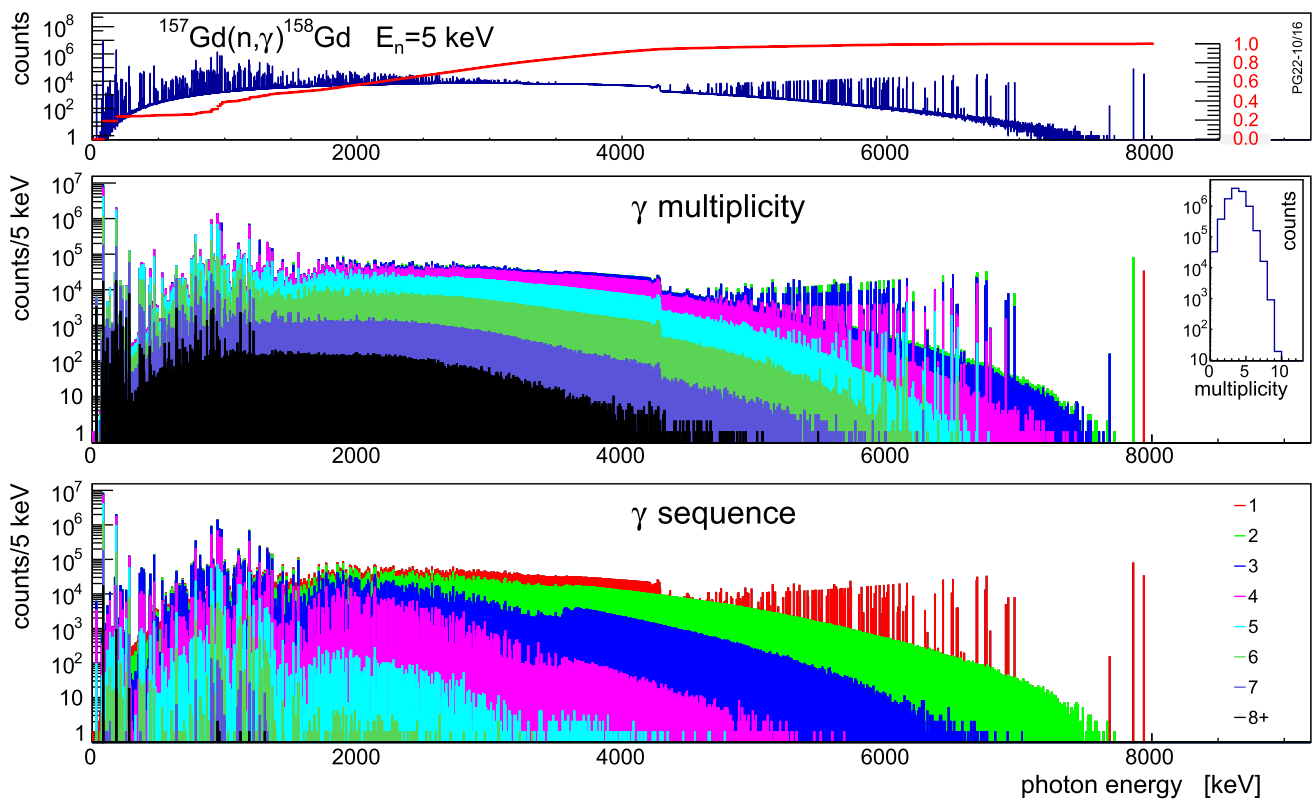


Fig. 14 γ -cascades from (n, γ) on ^{157}Gd employing the standard parameterization. Top: the total γ spectrum in ^{158}Gd and the running sum normalized to 1 (red line). Middle: the stacked spectrum for the

multiplicities M ; the inset shows the distribution of M . Bottom: the sequence of γ -quanta within the cascade. The color code is valid for the middle and bottom graph

only. For the comparison to the results of MAURINA the “ γ s only” spectrum (blue, bottom graph) is generated and also a second one, where cascades with a single 89 keV electron are added (magenta). Both spectra show the same asymmetry in the population of the first two states as seen in the $J^\pi = 2^-$ calculation by MAURINA. However, the multiplicity spectra are broader and the spectra exhibit some regular, fence-like structure. Possibly the theoretical states as well as the remnants from the binning of the continuum are the cause. The latter might pose no problem in simulations of setups with moderate energy resolution.

5.2 The (n, γ) reaction on ^{157}Gd

Figure 14 gives the results for the standard calculation on the (n, γ) reaction on ^{157}Gd . The spectra are rather similar to those for ^{155}Gd , except for the differences due to the different Q values [40]. The additional neutron is bound in ^{158}Gd by 7.936 MeV; the $^{157}\text{Gd}(n, 2n)$ threshold amounts to $Q(n, 2n) = 6.359$ MeV. Also the energy of the highest experimental level or equivalently the beginning of the continuum states at $E_c = 2.81$ MeV and 3.65 MeV for ^{156}Gd and ^{158}Gd ,

Table 5 The mean multiplicities M_m and cross sections $\sigma_{n\gamma}$ for the reaction $^{157}\text{Gd}(n, \gamma)^{158}\text{Gd}$ at 5 keV neutron energy. σ_n^p and σ_γ^p are the total production cross sections for neutrons and γ s, respectively. The cross sections are given in [b]. The lowest line gives the result when using only 108 excited states

Level dens.	f_{E1}	M_m	$\sigma_{n\gamma}$	σ_n^p	σ_γ^p
$E_n = 5$ keV					
KRK, π^d	3LO	4.29	5.39	17.22	23.14
KRK, π^c	3LO	4.31	5.68	16.93	24.49
KRK, π^d	ALO	4.47	5.65	16.96	25.24
1 exc., KRK, π^d	3LO	4.53	4.48	18.14	20.13
FG, π^d	3LO	5.00	4.50	13.83	39.51
108 exc., KRK, π^d	3LO	4.32	5.23	17.38	22.53

respectively, show their influence in the γ spectra differently in the ranges $0 - E_c$ and $S_n - E_c$.

The cross sections shown in Table 5 for various data sets do not differ that much between each other as compared to those for the reaction on ^{155}Gd . Still the results for the FG set are quite off in accordance with Fig. 3. It is interesting to realize that the capture cross section $\sigma_{n\gamma}$ for ^{157}Gd is lower by about a factor of 2 compared to that for ^{155}Gd , which is

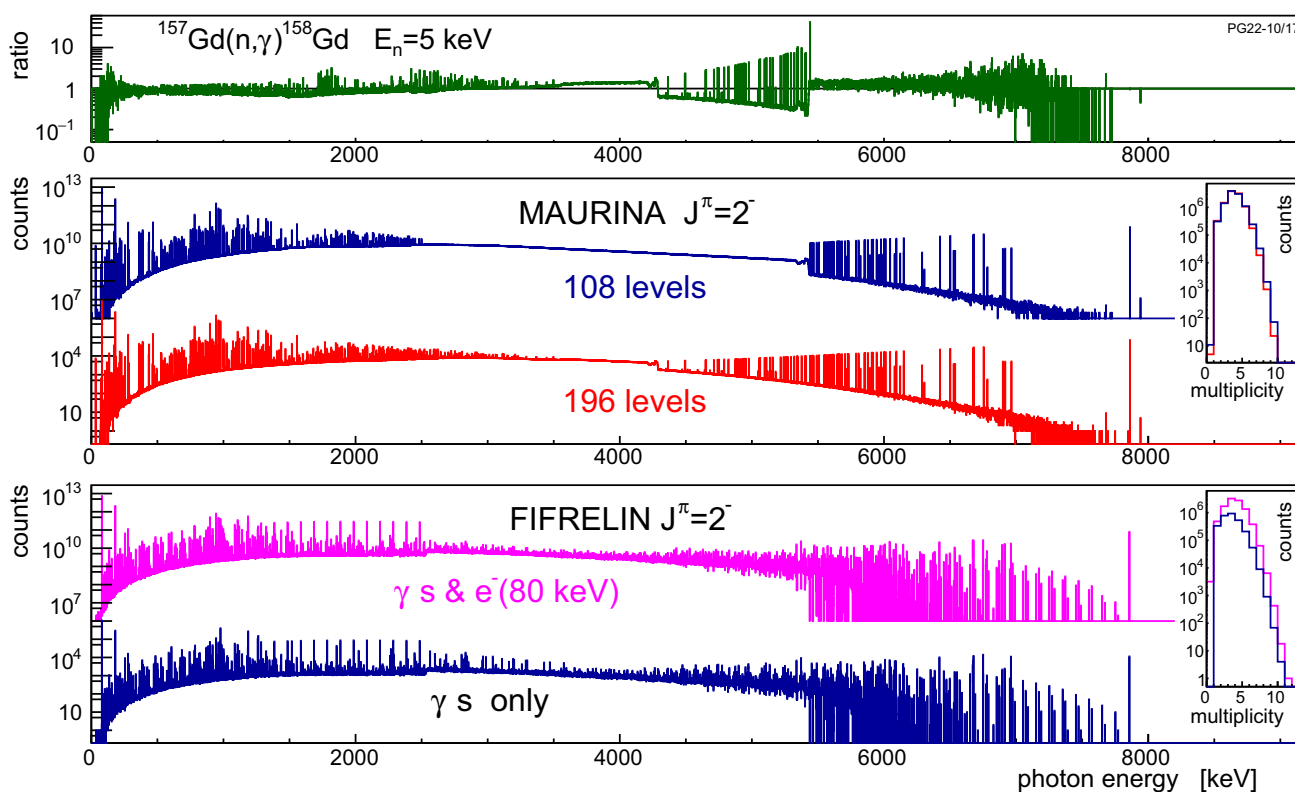


Fig. 15 γ -cascades from (n, γ) on ^{157}Gd separately for compound nucleus spin 2^- in comparison to those from FIFRELIN [8] and the respective multiplicities (insets). The binning amounts to 1 keV. Bottom: spectra for $J^\pi = 2^-$ by FIFRELIN selecting γ s only and (with

offset of 10^6) for γ s and the electrons from the first excited state at 80 keV; Middle: γ spectra for $J^\pi = 2^-$ by MAURINA with 108 and 196 experimental levels. Note the offset of 10^6 for the spectrum with 108 levels; Top: ratio of counts for spectra with 196 and 108 levels

quite opposite to the situation at thermal energies [1]. The mean multiplicities M_m are slightly lower in ^{158}Gd than in ^{156}Gd .

The results for higher neutron energies or cuts are too similar to those of ^{156}Gd described above, that a discussion is only warranted for specific setups with defined media and sensors. The only significant difference appears through the low number of experimental levels in the range from $E_x = 2.5$ to 3.65 MeV (see Fig. 3). When only the 108 experimental levels have been used instead of 196 and the level density formula being employed for higher excitation energies, the numbers do not diverge significantly (Table 5). The differences to the data set with 1 excited state only are more pronounced.

For a more sensitive comparison, the γ spectra are compared in Fig. 15 concentrating on $J^\pi = 2^-$ compound states only. The γ spectra for the data sets with the two different number of experimental levels are shown in the middle panel with a 1 keV binning. The differences become more clear in the their ratio dividing the full (196 levels) by the reduced (108 levels) spectrum (top panel). The strong differences at both end of the spectra are mostly due to small statistics. In general, deviations from unity are found at all energies with

the most prominent ones around 5 MeV by those γ s feeding discrete states directly.

The bottom panel shows the results by FIFRELIN again for γ s only and also when in addition the electron of 80 keV from the decay of the first excited state is added [8]. Just 37% of the cascades are made by γ transitions only, 64% contain a single electron of 80 keV, while 1% come with one electron of any energy, and 6.1% of the cascades contain between 2 and 4 electrons. The gross features of both spectra are rather similar. The regular pattern again are due to transitions between the theoretical states FIFRELIN assumes. The dominant direct transition from the capture state is to the first excited state due to the dominant $E1$ strength. There is no direct decay to the ground state in contrast to MAURINA where an albeit rather small fraction is observed.

The ratio of $J^\pi = 1^-/J^\pi = 2^-$ is similar to that for ^{156}Gd .

6 Conclusion

With the improved version of MAURINA, a code for Hauser-Feshbach calculations, cross sections and γ cascades have

been calculated in the epithermal energy region up to 10 MeV. The cascades provide more detailed information than the multiplicities alone. For a first test case calculations of neutron capture on the Gadolinium isotopes ^{155}Gd and ^{157}Gd has been chosen since these quantities will be helpful in the design of the veto properties of LEGEND-1000 or any other Gd-loaded sensors in rare-event searches. While MAURINA does not consider electron or β emission, its energy range is not restricted to the thermal region. This will be important for estimates considering background contributions by non-thermal neutrons produced from cosmic radiation in the vicinity of the sensitive materials.

Statistical model calculations are extremely dependent on the choice of the several models within and their parameters; and thus the results may be off easily by a factor of 2. In the present case the main interest is in the neutron energy range 1 keV to 1 MeV for neutron tagging. Thus, pre-compound emission or other direct reactions contribute negligibly. In this energy range only neutrons or γ s will be emitted reducing the number of active reaction channels further. The main groups of parameters have been discussed in this paper as they are (i) the multipole strength for the electro-magnetic transitions, (ii) the optical potentials for the relevant incoming and outgoing particles, and (iii) the discrete levels and level density parameters for the continuum. As explained in the specific subsections, the main parameters have been taken from successful calculations of other papers or adjusted to reproduce respective data. Unreasonable parameter sets lead to quite strong deviations as can be seen e.g. in Fig. 4 or Table 4 @ 1 MeV for $\sigma_{n\gamma}$ while σ_n^p changes much less and multiplicities M_m remain almost constant. Since not all parameters could be pinned down sufficiently, uncertainties for individual quantities are estimated to be around 25%. The overall uncertainty for cross sections is estimated to 15%. Relative quantities like the spectra from cascades will come with <10% uncertainty. At 10 MeV neutron energy more reaction channels will be open and pre-compound emission starts to contribute, thus increasing the uncertainties for the cross sections to 30–40%.

MAURINA can reproduce very well the experimental data. Close to 200 levels with their spin-parity have been provided. It was made certain, that in particular the $E1$ strength function and the level densities are consistent with literature. The cross sections in the epithermal region are larger for ^{155}Gd than for ^{157}Gd , which is opposite to the thermal region. However, both are significantly smaller at epithermic energies. Since within MAURINA specific compound states with defined J^π can be selected, the calculated cascades can be used in case of thermal neutron capture also because in both cases the energy transfer is negligible. Thus, γ cascades from resonant neutron capture can be emulated reliably. Differences in the cascades have been shown explicitly for $J^\pi = 1^-$ and 2^- , respectively. Specifically, direct population of low

lying levels is selective on the spin-parity of the compound state. While mostly the epithermic regime was investigated, some differences at higher energies are indicated. At 10 MeV other reaction channels have opened and the (n,γ) reaction becomes negligible.

The present HF calculations by MAURINA are compared to two other model calculations [8, 16, 17], respectively, without considering the specific modulation caused by the experimental setup. For the first analysis it is noted, that their HFB level densities are much larger than those inferred from experimental data. If the energy dependence of the various level density models would be identical then the cross sections would be different, but the γ cascades would just scale. However, due to the non-linear behavior of the density models, the γ cascades will differ. The FIFRELIN calculations [8] of the cascades are restricted to $J^\pi = 2^-$ resonances. In addition, they show fence-like effects due to the intermediate continuum states compared to a smooth continuum of MAURINA, which might be a nuisance in high resolution experiments. The comparison shows that the increased efforts for the more complex calculations pays off for high resolution experiments and detailed analyses.

The present input set for MAURINA allows for improved calculations in the epithermic energy range for both isotopes ^{155}Gd and ^{157}Gd and by combination for natural Gadolinium. The γ cascades can be used for realistic simulations of experimental setups. The large realistic set of discrete levels will be in particular useful for simulation of coincident experiments. For neutrons in the higher MeV range direct reaction contributions as inelastic scattering or one-nucleon transfers must be investigated. For natural Gadolinium additionally it might be necessary to consider contributions by the other even isotopes. Similar calculations will be performed for Germanium to support the suppression of possible background due to ^{77m}Ge in the upcoming $0\nu\beta\beta$ -experiment LEGEND.

Acknowledgements This work was supported by funds of the German Ministry for Education and Research (BMBF contract 05A20VT1). I am indebted to Brigitte Strohmaier, the de-facto scientific executor of Mario Uhl of the “Institut für Radiumforschung und Kernphysik”, Vienna - she saved and conserved all the code MAURINA and data files created by him in the years 1979–1995.

Data Availability Statement The manuscript has associated data in a data repository. [Authors’ comment: $10^7\gamma$ cascades following neutron capture on ^{155}Gd (Fig. 6) and ^{157}Gd (Fig. 14) each are available at <https://doi.org/10.5281/zenodo.7458654>.]

Open Access This article is licensed under a Creative Commons Attribution 4.0 International License, which permits use, sharing, adaptation, distribution and reproduction in any medium or format, as long as you give appropriate credit to the original author(s) and the source, provide a link to the Creative Commons licence, and indicate if changes were made. The images or other third party material in this article are included in the article’s Creative Commons licence, unless indicated otherwise in a credit line to the material. If material is not included in the article’s Creative Commons licence and your intended

use is not permitted by statutory regulation or exceeds the permitted use, you will need to obtain permission directly from the copyright holder. To view a copy of this licence, visit <http://creativecommons.org/licenses/by/4.0/>.

Funded by SCOAP³. SCOAP³ supports the goals of the International Year of Basic Sciences for Sustainable Development.

References

- S.F. Mughabhab, Atlas of neutron resonances vol. Fifth edition: resonance parameters and thermal cross sections, $Z = 1-100$ (Elsevier, Amsterdam, 2006)
- J.A. Edgington, A. Malik, B. Seligmann, G. Drexlin, V. Eberhard, K. Eitel, H. Gemmeke, G. Giorginis, W. Grandegger, M. Kleifges, J. Kleinfeller, P. Maschuw, P. Plischke, J. Rapp, F. Raupp, J. Wochele, J. Wolf, S. Wölflé, B. Zeitnitz, B. Bodmann, F. Burtak, E. Finckh, A. Glombik, T. Hanika, J. Hössl, W. Kretschmer, R. Meyer, S. Schilling, A. Dodd, N.E. Booth, Results from the KARMEN neutrino experiment. AIP Conf. Proc. **272**, 732 (1992). <https://doi.org/10.1063/1.43368>
- B. Armbruster, I.M. Blair, B.A. Bodmann, N.E. Booth, G. Drexlin, J.A. Edgington, C. Eichner, K. Eitel, E. Finckh, H. Gemmeke, J. Hössl, T. Jannakos, P. Jünger, M. Kleifges, J. Kleinfeller, W. Kretschmer, R. Maschuw, C. Oehler, P. Plischke, J. Reichenbacher, C. Ruf, M. Steidl, J. Wolf, B. Zeitnitz, Upper limits for neutrino oscillations $\nu \rightarrow \nu_e^-$ from muon decay at rest. Phys. Rev. D **65**, 112001 (2002). <https://doi.org/10.1103/PhysRevD.65.112001>
- Y. Aber et al. (Double Chooz Collaboration), Indication of reactor ν_e^- disappearance in the double CHOOZ experiment. Phys. Rev. Lett. **108**, 131801 (2012). <https://doi.org/10.1103/PhysRevLett.108.131801>
- J.K. Ahn et al. (RENO Collaboration), Observation of reactor electron antineutrinos disappearance in the RENO experiment. Phys. Rev. Lett. **108**, 191802 (2012). <https://doi.org/10.1103/PhysRevLett.108.191802>
- F.P. An et al. (Daya Bay Collaboration), Observation of electron-antineutrino disappearance at Daya Bay. Phys. Rev. Lett. **108**, 171803 (2012). <https://doi.org/10.1103/PhysRevLett.108.171803>
- H. Watanabe et al. (Super-Kamiokande Collaboration), First study of neutron tagging with a water cherenkov detector. Astropart. Phys. **31**, 320 (2009). <https://doi.org/10.1016/j.astropartphys.2009.03.002>
- H. Almazán, L. Bernard, A. Blanchet, A. Bonhomme, C. Buck, A. Chebboubi, P. del Amo Sanchez, I. El Atmani, J. Haser, F. Kandzia, S. Kox, L. Labit, J. Lamblin, A. Letourneau, D. Lhuillier, M. Lindner, O. Litaize, T. Materna, A. Minotti, H. Pessard, J.S. Réal, C. Roca, T. Salagnac, V. Savu, S. Schoppmann, V. Sergeeva, T. Soldner, A. Stutz, L. Thulliez, A. Vialat, Improved STEREO simulation with a new gamma ray spectrum of excited gadolinium isotopes using FIFRELIN. Eur. J. Phys. A **55**, 183 (2019). <https://doi.org/10.1140/epja/i2019-12886-y>
- D. Wenz, For the XENON Collaboration, Calibrating XENONnt and its novel water Cherenkov neutron-veto using tagged photons. In: 14th international conference on identification of dark matter, Vienna (2022)
- J.P. Stowell, S. Fargher, L.F. Thompson, A.M. Bown, P.M. Chadwick, Gadolinium loaded Cherenkov detectors for neutron monitoring in high energy air showers. JINST **17**, 02005 (2022). <https://doi.org/10.1088/1748-0221/17/02/T02005>
- J.-L. Shih, R.M. Brugger, Gadolinium as a neutron capture therapy agent. Med. Phys. **19**, 733 (1992). <https://doi.org/10.1118/1.596817>
- P. Kandlakunta, Gamma rays rejection in a gadolinium based neutron detector. PhD thesis, Ohio State University (2014)
- S. Agostinelli et al. (GEANT Collaboration), GEANT4—a simulation toolkit. Nucl. Instrum. Methods A **506**, 250 (2003). [https://doi.org/10.1016/S0168-9002\(03\)01368-8](https://doi.org/10.1016/S0168-9002(03)01368-8)
- T. Yano, Measurement of gamma-ray production from thermal neutron capture on gadolinium for neutrino experiments. Nucl. Instrum. Methods A **845**, 425 (2017). <https://doi.org/10.1016/j.nima.2016.06.084>
- I. Ou, Y. Yamada, T. Yano, T. Mori, T. Kayano, M. Sakuda, A. Kimura, H. Harada, Measurement of the energy, multiplicity and angular correlation of γ -rays from the thermal neutron capture reaction $Gd(n,\gamma)$ using JPARC-ANNRI. In: Origin of matter and evolution of galaxies 2013, vol. 1594, p. 351. AIP Conference Proceedings, Tsukuba (2014). <https://doi.org/10.1063/1.4874094>
- T. Tanaka, K. Hagiwara, E. Gazzola, A. Ali, I. Ou, T. Sudo, P.K. Das, M.S. Reen, R. Dhir, Y. Koshio, M. Sakuda, A. Kimura, S. Nakamura, N. Iwamoto, H. Harada, G. Collazuol, S. Lorenz, M. Wurm, W. Focillon, M. Gonin, T. Yano, Gamma-ray spectra from thermal neutron capture on gadolinium-155 and natural gadolinium. Prog. Theor. Exp. Phys. (2020). <https://doi.org/10.1093/ptep/ptaa015>
- K. Hagiwara, T. Yano, T. Tanaka, M.S. Reen, P.K. Das, S. Lorenz, I. Ou, T. Sudo, Y. Yamada, T. Mori, T. Kayano, R. Dhir, Y. Koshio, M. Sakuda, A. Kimura, S. Nakamura, N. Iwamoto, H. Harada, M. Wurm, W. Focillon, M. Gonin, A. Ali, G. Collazuol, Gamma-ray spectra from thermal neutron capture on gadolinium-157. Prog. Theor. Exp. Phys. (2019). <https://doi.org/10.1093/ptep/ptz002>
- B. Kutsenko, V. Ivantchenko, New Grant4 photonuclear cross-section model, Novosibirsk State University and CERN. CERN summer student program 2021 (2021). https://cds.cern.ch/record/2778865/files/Kutsenko_report.pdf
- M. Agostini et al. (GERDA Collaboration), Final results of GERDA on the search for neutrinoless double- β decay. Phys. Rev. Lett. **125**, 252502 (2020). <https://doi.org/10.1103/PhysRevLett.125.252502>
- N. Abgrall et al. (LEGEND Collaboration), The large enriched germanium experiment for neutrinoless double beta decay (LEGEND). AIP Conf. Proc. **1894**, 020027 (2017). <https://doi.org/10.1063/1.5007652>
- N. Burlak, For the LEGEND collaboration, Neutrinoless double beta decay search with LEGEND-200 experiment. In: Proceedings of 41st international conference on high energy physics—PoS (ICHEP2022), vol. 414, p. 602 (2022). <https://doi.org/10.22323/1.414.0602>
- C. Wiesinger, L. Pandola, S. Schönert, Virtual depth by active background suppression: revisiting the cosmic muon induced background of GERDA Phase II. Eur. Phys. J. C **78**, 597 (2018). <https://doi.org/10.1140/epjc/s10052-018-6079-3>
- M. Uhl, MAURINA—a computer code for nuclear reaction cross sections. IRK Report 87/12, Institut f. Radiumforschung und Kernphysik, Vienna (1987)
- M. Uhl, B. Strohmaier, STAPRE—a statistical model code with consideration of preequilibrium decay. IRK Report 76/01, Institut f. Radiumforschung und Kernphysik, Vienna (1976)
- W. Hauser, H. Feshbach, The inelastic scattering of neutrons. Phys. Rev. **87**, 366 (1952). <https://doi.org/10.1103/PhysRev.87.366>
- P.A. Moldauer, Statistics and the average cross section. Nucl. Phys. A **344**, 185 (1980). [https://doi.org/10.1016/0375-9474\(80\)90671-5](https://doi.org/10.1016/0375-9474(80)90671-5)
- W. Dilg, W. Schantl, H. Vonach, M. Uhl, Level density parameters for the back-shifted Fermi gas model in the mass range $40 < A < 250$. Nucl. Phys. A (1973). [https://doi.org/10.1016/0375-9474\(73\)90196-6](https://doi.org/10.1016/0375-9474(73)90196-6)
- T. von Egidy, D. Bucurescu, Systematics of nuclear level density parameters. Phys. Rev. C **72**, 044311 (2005). <https://doi.org/10.1103/PhysRevC.72.044311>

29. T. von Egidy, D. Bucurescu, Erratum: systematics of nuclear level density parameters. *Phys. Rev. C* **73**, 049901 (2006). <https://doi.org/10.1103/PhysRevC.73.049901>
30. S.K. Kataria, V.S. Ramamurthy, S.S. Kapoor, Semiempirical nuclear level density formula with shell effects. *Phys. Rev. C* **18**, 549 (1978). <https://doi.org/10.1103/PhysRevC.18.549>
31. M.T. McEllistrem, R.E. Shamu, J. Lachkar, G. Haouat, C. Lagrange, Y. Patin, J. Sigaud, F. Cocu, Deformation effects in neutron scattering from the sm isotopes. *Phys. Rev. C* **15**, 927 (1977). <https://doi.org/10.1103/PhysRevC.15.927>
32. G.S. Mani, M.A. Melkanoff, I. Iori, *Proton penetrabilities using an optical potential*. Technical report, CEA (1963). (**unpublished**)
33. C.M. Perey, F.G. Perey, Deuteron optical-model analysis in the range of 11 to 27 MeV. *Phys. Rev.* **132**, 755 (1963). <https://doi.org/10.1103/PhysRev.132.755>
34. F.D. Becchetti, G.W. Greenlees, General set of ^3He and triton optical-model potentials for $A > 40$, $E < 40$ MeV. In: *Polarization phenomena in nuclear reactions* ed. by H.H. Barschall, W. Haerberli, p. 682. the University of Wisconsin Press, Madison (1971)
35. L. McFadden, G.R. Satchler, Optical-model analysis of the scattering of 24.7 MeV alpha particles. *Nucl. Phys.* **84**, 177 (1966). [https://doi.org/10.1016/0029-5582\(66\)90441-X](https://doi.org/10.1016/0029-5582(66)90441-X)
36. C. Kalbach, The griffin model, complex particles and direct nuclear reactions. *Z. Phys. A* **283**, 401 (1977). <https://doi.org/10.1007/BF01417230>
37. J.M. Blatt, V.F. Weisskopf, *Theoretical Nuclear Theory* (Wiley, New York, 1952)
38. S. Goriely, S. Hilaire, A.J. Koning, Improved microscopic nuclear level densities within the Hartree–Fock–Bogoliubov plus combinatorial approach. *Phys. Rev. C* **78**, 064307 (2008). <https://doi.org/10.1103/PhysRevC.78.064307>
39. K. Wisshak, F. Voss, F. Käppeler, K. Guber, L. Kazakov, N. Kornilov, M. Uhl, G. Reffo, Stellar neutron capture cross sections of the gadolinium isotopes. *Phys. Rev. C* **52**, 2762 (1995). <https://doi.org/10.1103/PhysRevC.52.2762>
40. W.J. Huang, M. Wang, F.G. Kondev, G. Audi, S. Naimi, The Ame 2020 atomic mass evaluation (i). *Chin. Phys. C* **45**, 030003 (2021). <https://doi.org/10.1088/1674-1137/abddb0>
41. J. Kopecky, R.E. Chrien, Observation of the M1 giant resonance by resonance averaging in ^{106}Pd . *Nucl. Phys. A* **468**, 285 (1987). [https://doi.org/10.1016/0375-9474\(87\)90518-5](https://doi.org/10.1016/0375-9474(87)90518-5)
42. C.W. Reich, Nuclear data sheets for $A = 156$. *Nucl. Data Sheets* **113**, 2537 (2012). <https://doi.org/10.1016/j.nds.2012.10.003>
43. N. Nica, Nuclear data sheets for $A = 158$. *Nucl. Data Sheets* **141**, 1 (2017). <https://doi.org/10.1016/j.nds.2017.03.001>
44. D.W. Lang, The angular momentum dependence of the nuclear level density. *Nucl. Phys.* **77**, 545 (1966)
45. C. Kalbach, Exciton number dependence of the Griffin model two-body matrix element. *Z. Phys. A* **287**, 319 (1978). <https://doi.org/10.1007/BF01481712>
46. S.J. Friesenhahn, M.P. Fricke, D.G. Costello, W.M. Lopez, A.D. Carlson, Neutron resonance parameters and radiative capture cross sections of Gd from 3 eV to 370 keV. *Nucl. Phys. A* **146**, 337 (1970). [https://doi.org/10.1016/0375-9474\(70\)90729-3](https://doi.org/10.1016/0375-9474(70)90729-3)
47. V.S. Shorin, V.N. Kononov, E.D. Poletaev, Radiative capture cross-sections for neutrons in the 5–70 keV energy range, for isotopes of gadolinium and erbium. *Sov. J. Nucl. Phys.* **19**, 2 (1974)
48. J. Voignier, S. Joly, G. Grenier, D.M. Drake, L. Nilsson, Neutron capture cross section measurements of rubidium, yttrium, niobium, gadolinium, tungsten, platinum and thallium between 0.5 and 3.0 MeV. Technical report, CEA Saclay (1981)
49. Y. Nakajima, I. Tsubone, M. Mizumoto, Y. Furuta, M. Ohkubo, M. Sugimoto, Y. Kawarasaki, Neutron capture cross section measurements of ^{155}Gd and ^{157}Gd from 1.1 to 235 keV. *Ann. Nucl. Energy* **16**, 589 (1989). [https://doi.org/10.1016/0306-4549\(89\)90013-3](https://doi.org/10.1016/0306-4549(89)90013-3)
50. M. Mastromacro (n-TOF Collaboration), Cross section measurements of $^{155,157}\text{Gd}(n,\gamma)$ reactions at thermal and epithermal neutrons. *Eur. Phys. J. A* **55**, 9 (2019). <https://doi.org/10.1140/epja/i2019-12692-7>
51. W.C. Chung, T.I. Ro, G.N. Kim, S. Lee, M. Igashira, T. Ohsaki, Measurements of keV-neutron capture cross section and capture gamma-ray spectra of 155-Gd and 157-Gd. *J. Korean Phys. Soc.* **50**, 409 (2007). <https://doi.org/10.3938/jkps.50.409>
52. H. Beer, R.L. Macklin, The 151-Sm branching, a probe for the irradiation time scale of the s-process. *Astrophys. J.* **331**, 1047 (1988). <https://doi.org/10.1086/166621>
53. O. Litaize, O. Serot, L. Berge, Fission modelling with FIFRELIN. *Eur. Phys. J. A* **51**, 177 (2015). <https://doi.org/10.1140/epja/i2015-15177-9>